

Theoretical study of the absorption spectra of the sodium dimer

H.-K. Chung, K. Kirby, and J. F. Babb

*Institute for Theoretical Atomic and Molecular Physics, Harvard-Smithsonian Center for Astrophysics,
60 Garden Street, Cambridge, Massachusetts 02138*

(Received 15 August 2000; published 13 February 2001)

Absorption of radiation from sodium dimer molecular states correlating to $\text{Na}(3s)\text{-Na}(3s)$ is investigated theoretically. Vibrational bound and continuum transitions from the singlet $X^1\Sigma_g^+$ state to the first excited $A^1\Sigma_u^+$ and $B^1\Pi_u$ states and from the triplet $a^3\Sigma_u^+$ state to the first excited $b^3\Sigma_g^+$ and $c^3\Pi_g$ states are studied quantum-mechanically. Theoretical and experimental data are used to characterize the molecular properties, taking advantage of knowledge recently obtained from *ab initio* calculations, spectroscopy, and ultracold atom collision studies. The quantum-mechanical calculations are carried out for temperatures in the range from 1000 to 3000 K, and are compared with previous calculations and measurements where available.

DOI: 10.1103/PhysRevA.63.032516

PACS number(s): 33.70.Ca, 34.20.Mq, 33.20.-t, 52.25.Os

I. INTRODUCTION

Vast amounts of experimental spectroscopic data on the electronic states and rovibrational levels of the sodium dimer are available, and many theoretical studies have been performed. For example, Ref. [1] presented an extensive bibliography, summarizing a variety of work dating from 1874 to 1983. Nevertheless, recent developments in atom trapping and cold-atom spectroscopy have led to improved atomic and molecular data through combinations of measurements on cold collisions, photoassociation spectroscopy, and magnetic-field-induced Feshbach resonances [2–8]. Now that very reliable molecular data are available, accurate calculations of absorption spectra over a broad range of wavelengths at high temperatures become feasible.

Absorption spectra of the sodium dimer at visible wavelengths can be considered as an extension of collisional broadening of sodium resonance lines. Such line broadening data are of keen interest to the lighting industry, for example, in problems relating to high-pressure sodium lamps. In this context, absorption coefficients in absolute units for a gas of sodium atoms and molecules at temperatures from 1070 to 1470 K were measured over a range of wavelengths from 350 to 1075 nm by Schlejen *et al.* [9]. They performed semi-classical calculations involving relevant molecular singlet and triplet transitions, and those calculations can reproduce the overall shape of their absorption spectra but not finer-scale features such as rovibrational structures and satellites.

The present work is concerned with the absorption involving two ground Na ($3s$) atoms and a ground Na ($3s$) atom and an excited Na ($3p$) atom, corresponding to transitions from the $X^1\Sigma_g^+$ state to the $A^1\Sigma_u^+$ and $B^1\Pi_u$ states and the triplet transitions from the $a^3\Sigma_u^+$ state to the $b^3\Sigma_g^+$ and $c^3\Pi_g$ states. We assembled and evaluated the available data for the molecular system, and quantum mechanically calculated the absorption spectra at temperatures between 1000 and 3000 K. We present theoretical absorption spectra of the sodium dimer which show many of the detailed structures appearing in the experimental data by Schlejen *et al.* [9], and predict spectra at temperatures relevant to high-pressure sodium lamps.

II. ABSORPTION COEFFICIENTS

The thermally averaged absorption coefficients k_ν for molecular spectra at wavelength ν are obtained from the product of the thermally averaged cross sections and the molecular density [10]. In turn, the molecular density can be expressed in terms of the atomic density squared and the chemical equilibrium constant [11]. In the present study, we use the atomic density-independent reduced absorption coefficient k_ν/n_a^2 , where n_a is atomic density. Thus while the absorption coefficient has dimension $(\text{length})^{-1}$, the reduced absorption coefficient has dimension $(\text{length})^5$.

Assuming that $J' = J''$, where J'' and J' are, the initial and final rotational quantum numbers, respectively, the reduced absorption coefficients are derived for the four possible types of vibrational transitions, bound-bound (bb), bound-free (bf), free-bound (fb) and free-free (ff) between two electronic states. For the temperatures of interest here, $1000 \leq T \leq 3000$ K, this is a good approximation¹ since $J'' \sim J' \gg 1$. The radial wave function ϕ for a bound level or a continuum level is obtained from the Schrödinger equation for the relative motion of the nuclei,

$$\frac{d^2\phi(R)}{dR^2} + \left(2\mu E - 2\mu V(R) - \frac{J(J+1) - \Lambda^2}{R^2} \right) \phi(R) = 0, \quad (1)$$

where $V(R)$ is the potential for the relevant electronic state labeled by the projection Λ of the electronic orbital angular momentum on the internuclear axis, μ is the reduced mass of the nuclei, and E is the eigenvalue of the bound level or the continuum energy.

The bound-bound reduced absorption coefficient at frequency ν for transitions from a set of vibration-rotation lev-

¹For bound-bound transitions, one should take into account the rotational quantum number selection rules which give rise to the individual P , Q , and R branches. However, in the interest of brevity and without loss of generality, we present the approximate form obtained using $J' = J''$ in Eq. (2). One could generalize Eq. (2) to include Hönl-London factors properly accounting for branches.

els ($v''J''\Lambda''$) of the lower electronic state thermally populated at temperature T to a set of vibration-rotation levels of the upper electronic state ($v'J'\Lambda'$) is [10,12–14]

$$\begin{aligned} \frac{k_\nu^{bb}}{n_a^2} &= \frac{C(\nu)}{h} f(k_B T) \exp(D_e/k_B T) \\ &\times \sum_{v''J''} \sum_{v'} \omega_{J''}(2J''+1) \exp(-E_{v''J''}/k_B T) \\ &\times \langle \phi_{v''J''\Lambda''} | D(R) | \phi_{v'J'\Lambda'} \rangle^2 g(\nu - \bar{\nu}), \end{aligned} \quad (2)$$

where ν is the frequency, $\bar{\nu}$ is the transition energy of the bound-bound transition,

$$C(\nu) = \frac{(2 - \delta_{0,\Lambda'+\Lambda''})}{2 - \delta_{0,\Lambda''}} \frac{8\pi^3 \nu}{3c}, \quad (3)$$

and [15]

$$f(k_B T) = \frac{(2S_m + 1)}{(2S_a + 1)^2} \left[\frac{h^2}{2\pi\mu k_B T} \right]^{3/2}. \quad (4)$$

S_m and S_a are spin multiplicities for the Na_2 molecule and the Na atom, respectively, and k_B is the Boltzmann constant. The line-shape function $g(\nu - \bar{\nu})$ is replaced by $1/\Delta\nu$, and in evaluating Eq. (2) at some ν_i on the discretized frequency interval, all transitions within the frequency range $\nu_i - \frac{1}{2}\Delta\nu$ to $\nu_i + \frac{1}{2}\Delta\nu$ are summed to give a value $k^{bb}(\nu_i)/n_a^2$. The nuclear spin statistical factor ω_J for ${}^7\text{Na}_2$ with $I = \frac{3}{2}$ is as follows; for singlet states, $[I/(2I+1)] = \frac{3}{8}$ for even J and $[(I+1)/(2I+1)] = \frac{5}{8}$ for odd J , and for triplet states, it is $\frac{3}{8}$ for odd J and $\frac{5}{8}$ for even J .

The bound-free reduced absorption coefficient for transitions from a set of bound levels of the lower electronic state ($v''J''\Lambda''$) to all levels ($\epsilon'J'\Lambda'$) of the upper electronic state that can be accessed by absorption of a photon at frequency ν is

$$\begin{aligned} \frac{k_\nu^{bf}}{n_a^2} &= C(\nu) f(k_B T) \exp(D_e/k_B T) \times \sum_{v''J''} \omega_{J''}(2J''+1) \\ &\times \exp(-E_{v''J''}/k_B T) \langle \phi_{v''J''\Lambda''} | D(R) | \phi_{\epsilon'J'\Lambda'} \rangle^2. \end{aligned} \quad (5)$$

The continuum wave function is energy normalized. For a free-bound transition and free-free transition, respectively,

$$\begin{aligned} \frac{k_\nu^{fb}}{n_a^2} &= C(\nu) f(k_B T) \sum_{v'J'} \omega_{J'}(2J'+1) \\ &\times \exp(-\epsilon''/k_B T) \langle \phi_{\epsilon''J''\Lambda''} | D(R) | \phi_{v'J'\Lambda'} \rangle^2 \end{aligned} \quad (6)$$

and

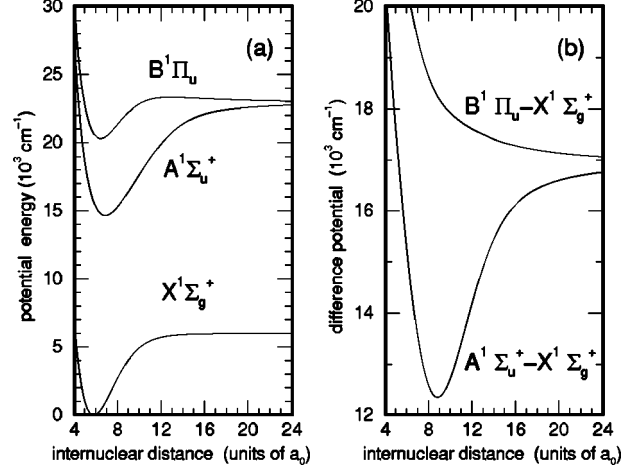


FIG. 1. (a) Adopted potentials $V(R)$ for the $X^1\Sigma_g^+$, $A^1\Sigma_u^+$, and $B^1\Pi_u$ electronic states. (b) Difference potentials $V_{B^1\Pi_u}(R) - V_{X^1\Sigma_g^+}(R)$ and $V_{A^1\Sigma_u^+}(R) - V_{X^1\Sigma_g^+}(R)$.

$$\begin{aligned} \frac{k_\nu^{ff}}{n_a^2} &= C(\nu) f(k_B T) \sum_{J'} \int d\epsilon' \omega_{J''}(2J''+1) \\ &\times \exp(-\epsilon''/k_B T) \langle \phi_{\epsilon''J''\Lambda''} | D(R) | \phi_{\epsilon'J'\Lambda'} \rangle^2. \end{aligned} \quad (7)$$

III. MOLECULAR DATA

Certain potential-energy curves of Na_2 are known more accurately than others. While the potentials constructed here may be far from spectroscopic accuracy, they are sufficient for the present high temperature broadband study. The adopted $X^1\Sigma_g^+$, $A^1\Sigma_u^+$, and $B^1\Pi_u$ potentials and the differences of the upper potentials and the lower $X^1\Sigma_g^+$ potential (difference potentials or transition energies) are plotted in Fig. 1. The adopted $a^3\Sigma_u^+$, $b^3\Sigma_g^+$, and $c^3\Pi_g$ potentials and the difference potentials are plotted in Fig. 2. In the remainder of the section details on the construction of the potentials are given. We use atomic units throughout.

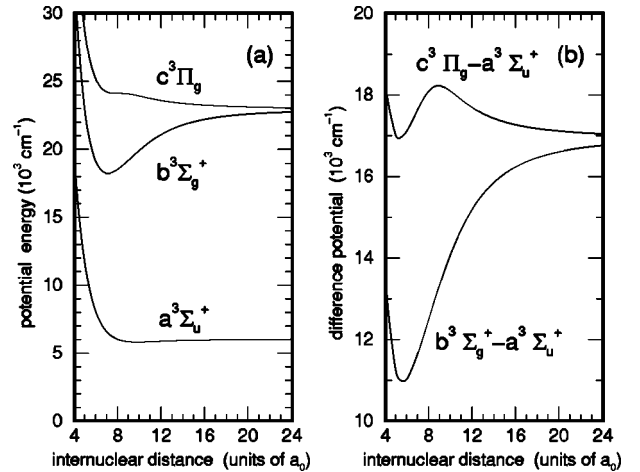


FIG. 2. (a) Adopted potentials $V(R)$ for the $a^3\Sigma_u^+$, $b^3\Sigma_g^+$ and $c^3\Pi_g$ states. (b) Difference potentials $V_{b^3\Sigma_g^+}(R) - V_{a^3\Sigma_u^+}(R)$ and $V_{c^3\Pi_g}(R) - V_{a^3\Sigma_u^+}(R)$.

A. $X^1\Sigma_g^+$ potential

For $R < 4a_0$, we adopted a short-range form $a \exp(-bR)$, with $a = 2\,702\,514.0 \text{ cm}^{-1}$ and $b = 2.797\,131 \text{ \AA}^{-1}$ as given by Zemke and Stwalley [16]. Over the range of $4a_0 < R < 30a_0$ we used the Inverse Perturbation Analysis (IPA) potential given by van Abeelen and Verhaar [7] which is consistent with data from photoassociation spectroscopy, molecular spectroscopy, and magnetic-field-induced Feshbach resonances in ultra-cold atom collisions. For the long-range form, we used

$$-C_6/R^6 - C_8/R^8 - C_{10}/R^{10} - AR^{(7/2)\alpha-1} \exp(-2\alpha R), \quad (8)$$

where $C_6 = 1\,561$ [2], $C_8 = 111\,877$, $C_{10} = 11\,065\,000$ [17], $A = \frac{1}{80}$, and $\alpha = 0.626$ [7,18]. To fit the very accurate dissociation energy, $6\,022.0286(53) \text{ cm}^{-1}$, recently measured by Jones *et al.* [19], a point at the potential minimum $5.819\,460a_0$ was added. The short- and long-range data were smoothly connected to the IPA values. Vibrational eigenvalues calculated with our adopted potential agree for $v \leq 44$ to within 0.1 cm^{-1} with published Rydberg-Klein-Rees (RKR) values [16]. Our final potential yielded an s -wave scattering length of $15a_0$ in satisfactory agreement with the accepted value of $(19.1 \pm 2.1)a_0$ [7].

B. $A^1\Sigma_u^+$ potential

We used *ab initio* calculations given by Konowalow *et al.* [20] for values of R over the range $3.8a_0 < R < 4.75a_0$. We combined the RKR potential values over the range $2.522\,19 \text{ \AA} < R < 7.204\,14 \text{ \AA}$ given by Gerber and Möller [21] with the RKR potential values over the range of $7.260\,536 \text{ \AA} < R < 261.327\,403 \text{ \AA}$ given by Tiemann, Knöckel, and Richling [22,23]. The data were connected to the long-range form,

$$-C_3/R^3 - C_6/R^6 - C_8/R^8, \quad (9)$$

with the values of $C_3 = 12.26$, $C_6 = 4\,094$, and $C_8 = 702\,500$ [24]. For $R < 3.8a_0$, the form $a \exp(-bR) + c$ was used with the parameters $a = 0.9532$, $b = 0.5061$, and $c = 0.104696$ computed to smoothly connect to the RKR points. The adopted potential yields a value of $D_e = 8\,297.5 \text{ cm}^{-1}$ using $T_e = 14\,680.682 \text{ cm}^{-1}$ [21] and the atomic asymptotic energy of $16\,956.172 \text{ cm}^{-1}$ [25]. The calculated eigenvalues reproduce the input RKR values to within 0.4 cm^{-1} . For the transition frequencies measured by Verma, Vu, and Stwalley [26] and by Verma *et al.* [1] over a range of vibrational bands we find typical agreement to about 0.4 cm^{-1} for J' values up to 50 increasing to 1 cm^{-1} for $J' = 87$. We also have good agreement with less accurate measurements by Itoh *et al.* [27]. One precise transition-energy measurement is available: In a determination of the dissociation energy of the sodium molecule, Jones *et al.* [19] measured the value $18762.3902(30) \text{ cm}^{-1}$ for the $v' = 165$, $J' = 1$ to $v'' = 31$, $J'' = 0$ transition energy. Our value of $18762.372 \text{ cm}^{-1}$ is in excellent agreement.

C. $B^1\Pi_u$ potential

The RKR potential of Kusch and Hessel [28] was used² over the range of $2.655\,5671 \text{ \AA} < R < 5.173\,5134 \text{ \AA}$. For the values of R in the ranges $2.581 \text{ \AA} < R < 2.646\,0268 \text{ \AA}$ and $5.251\,9184 \text{ \AA} < R < 11.0 \text{ \AA}$, we took the potential values from Tiemann [30]. We also took his long-range form,

$$C_3/R^3 - C_6/R^6 + C_8/R^8 - a \exp(-bR), \quad (10)$$

with $C_3 = 6.1486$, $C_6 = 6\,490.5$, $C_8 = 868\,135.2$, $a = 23.7011$, and $b = 0.7885$. For $R < 2.581 \text{ \AA}$, the form $a \exp(-bR) + c$ was used with the values $a = 14.973\,32$, $b = 1.429\,83$, and $c = 0.012\,1935$ chosen to give a smooth connection with the data from Tiemann.

The $B^1\Pi_u$ potential exhibits a barrier that has been studied extensively [21,29–31] and the maximum value occurs around $R = 13a_0$ (6.9 \AA) as shown in Fig. 1. We took $D_e = 2\,676.16 \text{ cm}^{-1}$ using $T_e = 20\,319.19 \text{ cm}^{-1}$ from Kusch and Hessel [28] and the barrier energy 371.93 cm^{-1} measured from dissociation given by Tiemann [30]. The calculated energy $23\,393.524 \text{ cm}^{-1}$ of the $v' = 31$, $J' = 42$ state with respect to the $X^1\Sigma_g^+$ state potential minimum compares well to the measured value: $23\,393.650 \text{ cm}^{-1}$. Quasibound levels from $v' = 24$ to $v' = 33$ for the several J' values observed by Vedder *et al.* [32] are reproduced to within 0.1 cm^{-1} and calculated transition frequencies compare well, to within 0.5 cm^{-1} , with those measured by Camacho *et al.* [33].

D. $a^3\Sigma_u^+$ potential

RKR potentials are available from Li, Rice, and Field [34] and Friedman-Hill and Field [35] and a hybrid potential was constructed by Zemke and Stwalley [16] using various available data. An accurate *ab initio* study was carried out by Gutowski [3] for R values between 2 and 12.1 \AA and the resulting potential has well depth 176.173 cm^{-1} and equilibrium distance 5.204 \AA .

Our adopted potential consists of Gutowski's potential connected to the long-range form given in Eq. (8) with the values for C_6 , C_8 , C_{10} , and α the same as for the $X^1\Sigma_g^+$ state, but with $A = -\frac{1}{80}$. For $R < 2 \text{ \AA}$ the short-range form $a \exp(-bR)$ was used with $a = 1.4956$ and $b = 0.79438$ chosen to smoothly connect to the *ab initio* data. Our adopted potential yields an s -wave scattering length of $65a_0$ in agreement with the value 65.3 ± 0.9 of van Abeelen and Verhaar [7]. Recently, a potential alternative to Gutowski's was presented by Ho *et al.* [36]. For the present study the two potentials are comparable.

E. $b^3\Sigma_g^+$ and $c^3\Pi_g$ potentials

We are unaware of empirical excited-state triplet potentials, but *ab initio* calculations are available from Magnier

²For this reference, we correct an apparent typographical error of $4.309\,78 \text{ \AA}$ with $4.339\,78 \text{ \AA}$ obtained by comparison with the RKR potential of Demtröder and Stock [29].

et al. [37], Jeung [38], and Konowalow *et al.* [20]. Comparing the available potentials, we found for the $b^3\Sigma_g^+$ state that the experimentally [39] determined T_e of 18 240.5 cm^{-1} and D_e of 4 755 cm^{-1} are closest to Magnier's calculated values (T_e of 18 117 cm^{-1} and D_e of 4 740.7 cm^{-1}) compared with Jeung's (T_e of 18 400 cm^{-1} and D_e of 4 702.4 cm^{-1}) and Konowalow *et al.*'s (D_e of 4 599 cm^{-1}). Also, we found Magnier's potential gave the best agreement with experimental measurements [40] of the term differences of the $a^3\Sigma_u^+(v'') \rightarrow b^3\Sigma_g^+(v')$ vibrational transitions. For the $b^3\Sigma_g^+$ state, and in the absence of experimental data for the $c^3\Pi_g$ potential, we adopted Magnier's calculated potentials over the range of R values $5a_0 < R < 52a_0$. Over the range of R values $4.25a_0 < R < 5a_0$, we used potentials by Konowalow *et al.* [20]. For the $b^3\Sigma_g^+$ and $c^3\Pi_g$ adopted potentials, the long-range form was taken from Marinescu and Dalgarno [24] for $R > 52a_0$ and for $R < 4.25a_0$, we used the form $a \exp(-bR)$ where the values are $a = 55.7864$ and $b = 1.75934$ for the $b^3\Sigma_g^+$ potential and $a = 2.67691$ and $b = 0.91547$ for the $c^3\Pi_g$ potential.

F. Transition dipole moment functions

We used for the singlet transitions the *ab initio* calculations of Stevens *et al.* [41] over the range $2a_0 < R < 12a_0$. For $R > 12$ the transition dipole moment functions were approximated by $a + b/r^3$, where $a = 3.5864$ and $b = 284.26$ for $X^1\Sigma_g^+ \rightarrow A^1\Sigma_u^+$ transitions and $a = 3.5017$ and $b = -142.13$ for $X^1\Sigma_g^+ \rightarrow B^1\Pi_u$ transitions. The parameter values for a were selected to match the short-range parts and those for b were from Marinescu and Dalgarno [24]. The $X^1\Sigma_g^+ \rightarrow A^1\Sigma_u^+$ dipole moment function was scaled with a factor of 1.008, as discussed in Sec. IV A below. For the triplet transitions the *ab initio* calculations of Konowalow *et al.* [42] were used over the range $4a_0 < R < 100a_0$.

IV. RESULTS

A. Lifetimes

In order to evaluate our assembled potential-energy and transition dipole-moment data, we calculated lifetimes of rovibrational levels of the $A^1\Sigma_u^+$ and $B^1\Pi_u$ states and compared with prior studies. Lifetimes for levels of the $A^1\Sigma_u^+$ state have been measured [26,43–45] and calculated [26,46]. In Fig. 3 we present a comparison of rotationally resolved lifetimes for levels of the $A^1\Sigma_u^+$ state measured by Baumgartner *et al.* [45] with the present calculations. In evaluating the lifetimes, we used the procedures described in Ref. [10]. The transition dipole moment function of Ref. [41] was multiplied by a factor of 1.008 providing good agreement with the lifetime measurements of Baumgartner *et al.* [45]. Our calculations are also in good agreement with the rotationally unresolved measurement of Ducas *et al.* [43] and the calculations using different molecular data by Pardo [46].

Rotationally resolved lifetimes for the $B^1\Pi_u$ state were measured by Demtröder *et al.* [47] and calculated by Camacho *et al.* [48]. Demtröder *et al.* found that the lifetimes for the $B^1\Pi_u$ state are sensitive to the slope of the transition

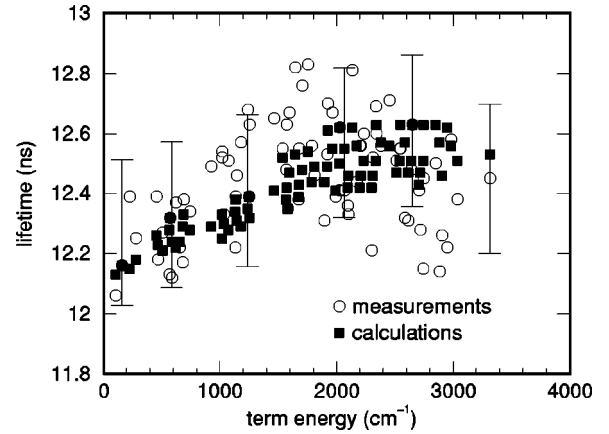


FIG. 3. Comparisons of calculated lifetimes of $A^1\Sigma_u^+$ rovibrational levels with experimental measurements [45].

dipole moment function in the range of internuclear separation from, roughly, $4a_0 < R < 10a_0$ and they obtained an empirical value for the function that we found to be in good agreement with the transition dipole moment function of Stevens *et al.* [41]. Using the transition dipole moment function of Stevens *et al.*, in turn, we find good agreement between our calculated lifetimes and experimental lifetime measurements [47], as shown in Fig. 4. The *ab initio* dipole moment of Konowalow *et al.* [42] was found not to reproduce the experimental lifetimes. Our calculations agree with those previous calculations [48] within quoted experimental uncertainties.

B. Absorption coefficients

Absorption spectra in the far-line wings of the $\text{Na}(3s)\text{-Na}(3p)$ resonance lines are investigated in terms of singlet and triplet molecular transitions. The blue wing consists of absorption from $X^1\Sigma_g^+ \rightarrow B^1\Pi_u$ and $a^3\Sigma_u^+ \rightarrow c^3\Pi_g$ transitions, and the red wing from $X^1\Sigma_g^+ \rightarrow A^1\Sigma_u^+$ and $a^3\Sigma_u^+ \rightarrow b^3\Sigma_g^+$ transitions. There are few experimental studies [9,14,49], and that of Schlejen *et al.* [9] is most relevant

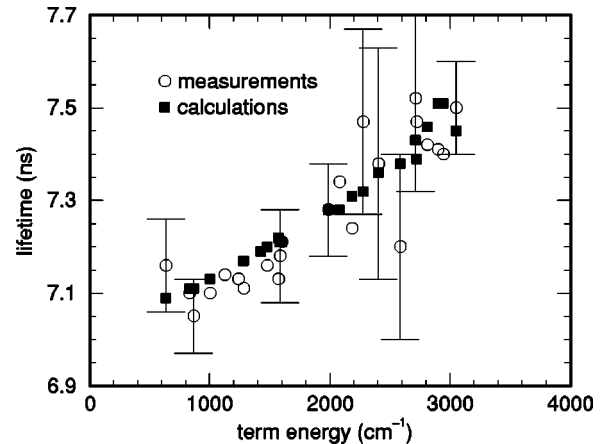


FIG. 4. Comparisons of calculated lifetimes of $B^1\Pi_u$ rovibrational levels with experimental measurements [47].

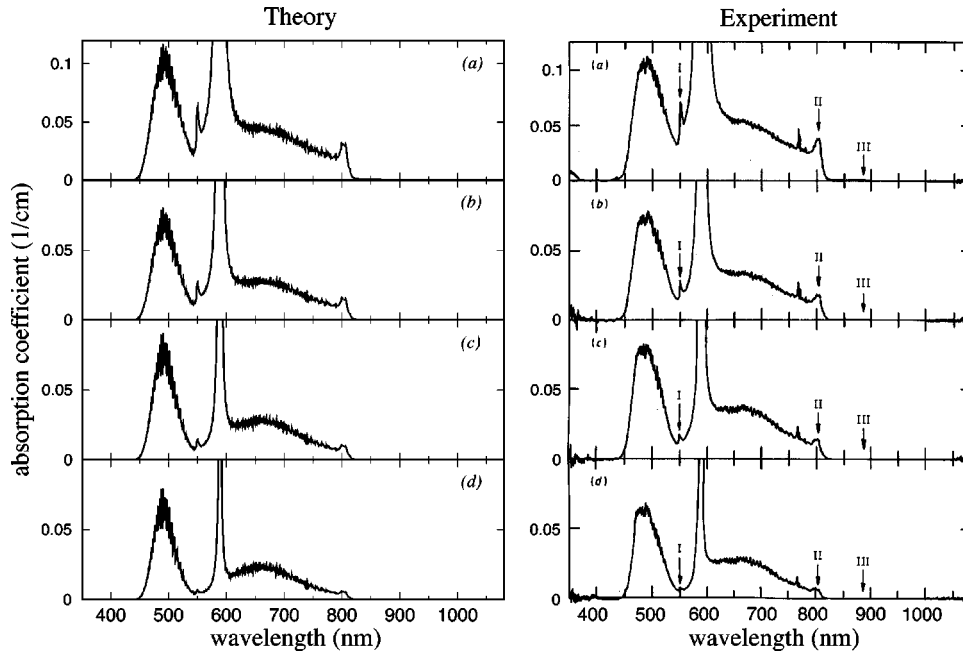


FIG. 5. Comparisons of the present theoretical (left side) and the experimental [9] (right side) absolute values of the absorption coefficient for the four temperatures (a) 1470 K, (b) 1340 K, (c) 1180 K, and (d) 1070 K. The calculations were performed with a bin size $\Delta\nu=10\text{ cm}^{-1}$. For the experimental data the symbols I, II, and III indicate, respectively, the $a^3\Sigma_u^+ \rightarrow c^3\Pi_g$, $X^1\Sigma_g^+ \rightarrow A^1\Sigma_u^+$, and $a^3\Sigma_u^+ \rightarrow b^3\Sigma_g^+$ satellites. (The features between 770 and 790 nm are due to potassium and rubidium impurities.) The experimental data were reproduced from Fig. 5 of Schlejen *et al.* [9] with permission from the Institute of Physics and the authors.

to our work. In this section, we compare our calculated absorption coefficients with the measurements of Schlejen *et al.* [9].

The theoretical spectra are assembled from four molecular band spectra over the wavelength range 450–1000 nm excluding the region 589 ± 2 nm around the atomic resonance lines. The far-line wings are calculated using Eqs. (2)–(7), with the data from Sec. III. In the calculations, all the vibrational levels including quasibound levels with rotational quantum numbers up to 250 are included.³ The maximum internuclear distance that is used for integration of the transition dipole matrix element is approximately $100a_0$, and the Numerov integration used to obtain the energy-normalized continuum wave function is carried out to $100a_0$, at which the wave function is matched to its asymptotic form. In order to simulate the experiment, it is sufficient to use a 10 cm^{-1} bin size $\Delta\nu$ for the approximate line shape function in Eq. (2). Results for absolute absorption coefficients were computed with the quoted atomic densities and temperatures of Schlejen *et al.* [9]. The corresponding theoretical calculations and experimental measurements are compared in Fig. 5. The spectra show clearly that, as temperature increases, certain satellite features grow more apparent at 551.5 and 804 nm. These satellites will be discussed in greater detail later in this section. Our calculations reproduce fine-scale rovibrational features present but unresolved in the measurements of Ref. [9].

We also have calculated reduced absorption coefficients at temperatures up to 3000 K using the bin size $\Delta\nu$ of 1 cm^{-1} for Eq. (2). The contributions of the four molecular bands to the reduced absorption coefficients are shown in Fig. 6 for three temperatures 1000, 2000, and 3000 K. As can

be seen by comparing columns (a) and (b) in Fig. 6, the singlet transitions contribute more to the reduced absorption coefficients in the far-line wings and the triplet transitions contribute more near the atomic resonance lines. We found that for singlet transitions bound-bound and bound-free transitions are dominant over free-bound and free-free transitions for the temperature range $T\leq 3000\text{ K}$, thus accounting for the “grassy” structure in Fig. 6(a). However, the free-bound and free-free contributions increase rapidly with temperature. In contrast to the singlet transitions, the triplet transitions arise mainly from free-bound and free-free transitions due to the shallow well of the initial $a^3\Sigma_u^+$ state. Hence, the reduced absorption coefficients in Fig. 6(b) do not exhibit much structure. Because the density of bound molecules decreases rapidly with increasing temperature, the reduced absorption coefficient in the line wings due to the singlet transitions also decreases rapidly with increasing temperature. It should be noted that the scale of the reduced absorption coefficient at 1000 K is two orders of magnitude larger than the scale shown for $T=2000$ and 3000 K.

Woerdman and De Groot [49] derived the reduced absorption coefficient at 2000 K from a discharge spectra. The measured values of $5\pm 1\times 10^{-37}\text{ cm}^5$ at 500 nm and $10\pm 1\times 10^{-37}\text{ cm}^5$ at 551.5 nm are well reproduced by our values of 5×10^{-37} and $11\times 10^{-37}\text{ cm}^5$, respectively calculated with a bin size $\Delta\nu$ of 5 cm^{-1} simulating the experimental resolution obtained by Woerdman and De Groot [49].

The molecular absorption spectra contain “satellite” features around the energies where the difference potentials possess local extrema [50,51]. For Na_2 the satellite frequencies were studied [9,14,49,52], and the energies calculated using *ab initio* methods [42]. In the present work, we investigate the satellites arising from $a^3\Sigma_u^+ \rightarrow c^3\Pi_g$, $X^1\Sigma_g^+ \rightarrow A^1\Sigma_u^+$, and $a^3\Sigma_u^+ \rightarrow b^3\Sigma_g^+$ transitions with measured maximum intensities at the wavelengths 551.5, 804, and 880 nm labeled, respectively, I, II, and III in Fig. 5. The calculated extrema of the difference potentials adopted in the present study occur at

³We accounted for rotational branches in the calculation for the bound-bound transitions in $X^1\Sigma_g^+ \rightarrow A^1\Sigma_u^+$ and $X^1\Sigma_g^+ \rightarrow B^1\Pi_u$ bands.

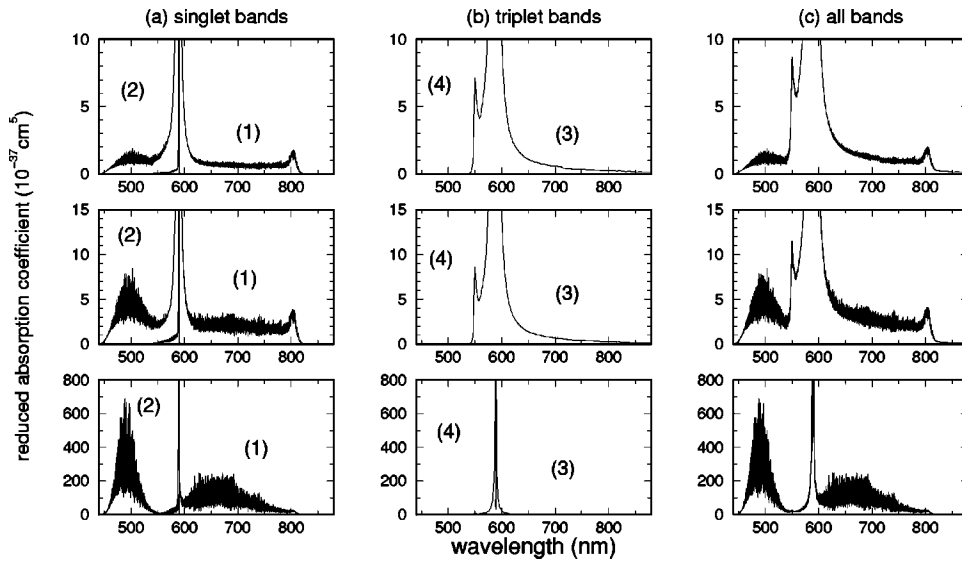


FIG. 6. Contributions to the reduced absorption coefficient at 1000 K (bottom plots), 2000 K (center plots), and 3000 K (top plots) from molecular band radiation from (a) the singlet bands, $X^1\Sigma_g^+ \rightarrow A^1\Sigma_u^+(1)$ and $X^1\Sigma_g^+ \rightarrow B^1\Pi_u(2)$ transitions; and (b) the triplet bands, $a^3\Sigma_u^+ \rightarrow b^3\Sigma_g^+(3)$ and $a^3\Sigma_u^+ \rightarrow c^3\Pi_g(4)$ transitions. The total of the singlet and triplet bands is shown in (c). Note that the scale for the reduced absorption coefficient at 1000 K is very much greater than the scale at 2000 and 3000 K. The calculations were performed with a bin size $\Delta\nu=1 \text{ cm}^{-1}$.

wavelengths at 548, 809, and 910 nm; however, in the quantum-mechanical approach there is no well-defined singularity.

We can use the quantum-mechanical theory to study satellite features in more detail and as a function of temperature. In Fig. 7 we show calculated reduced absorption coefficients at three temperatures for the $a^3\Sigma_u^+ \rightarrow c^3\Pi_g$ and $X^1\Sigma_g^+ \rightarrow A^1\Sigma_u^+$ transitions. The rich rovibrational structure in the $X^1\Sigma_g^+ \rightarrow A^1\Sigma_u^+$ satellite feature arises because the dominant contributions are from bound-bound transitions; the structure is not reproduced by semiclassical theories [9]. In contrast, the smooth, structureless $a^3\Sigma_u^+ \rightarrow c^3\Pi_g$ satellite feature is due mainly to free-free transitions, and, conse-

quently, the decrease of the satellite intensity with temperature is less severe. The slight discrepancy between the calculated wavelength of 550 nm and the measured wavelength of 551.5 nm [49,53,54] for the peak intensity is probably due to remaining uncertainties in the triplet potentials [36].

The $a^3\Sigma_u^+ \rightarrow b^3\Sigma_g^+$ satellite is far weaker in intensity at $T \leq 3000 \text{ K}$ than the $X^1\Sigma_g^+ \rightarrow A^1\Sigma_u^+$ and $a^3\Sigma_u^+ \rightarrow c^3\Pi_g$ satellites. It arises primarily from free-bound transitions. The population density of atom pairs with high continuum energies in the initial $a^3\Sigma_u^+$ state increases with temperature [see Eq. (6)], and more rovibrational levels in the $b^3\Sigma_g^+$ state are accessible through absorption of radiation, as can be seen from the potential curves shown in Fig. 2(a). As a result, this satellite feature exhibits an increase in intensity with temperature. In Fig. 8 our calculated absorption coefficients for temperatures 1000, 1500, 2000, and 3000 K are plotted. The

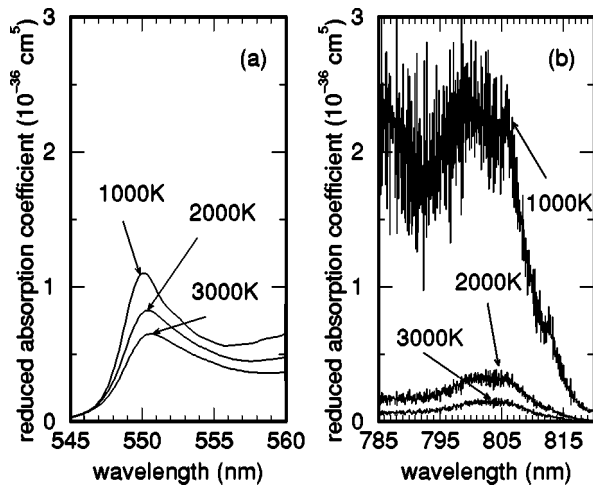


FIG. 7. (a) Calculated reduced absorption coefficients for the $a^3\Sigma_u^+ \rightarrow c^3\Pi_g$ satellite for three temperatures. (b) Calculated reduced absorption coefficients for the $X^1\Sigma_g^+ \rightarrow A^1\Sigma_u^+$ satellite for three temperatures.

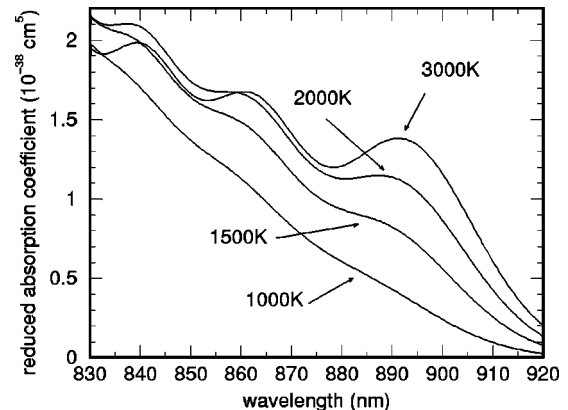


FIG. 8. Reduced absorption coefficients near satellite structures from $a^3\Sigma_u^+ \rightarrow b^3\Sigma_g^+$ bands for four temperatures. Note that the scale is two orders of magnitude smaller than in Fig. 7.

satellite feature intensity was measured at 1470 K by Schlejen *et al.* [9], and they observed a primary peak at 880 nm and a secondary peak at 850 nm, compared to our calculated values at 1500 K of 890 and 860 nm, respectively. The 10-nm discrepancy in both peaks is probably a result of uncertainties in the short range parts of our adopted $a^3\Sigma_u^+$ and $b^3\Sigma_g^+$ potentials. Our calculations also demonstrate that the wavelengths of the peaks change with temperature (see Fig. 8), and that the primary peak from quantum-mechanical calculations is less prominent than that obtained from semiclassical calculations exhibited in Figs. 6(c) and 6(d) of Schlejen *et al.* [9]. Nonetheless, the magnitude of our calculated reduced absorption coefficients appear to be in excellent agreement with the reduced absorption coefficients interpolated from Figs. 6(a) and 6(b) of Schlejen *et al.* [9] using their quoted Na densities.

V. CONCLUSIONS

We have carried out quantum-mechanical calculations of the reduced absorption coefficients in sodium vapor at high

temperatures. Using accurate molecular data, good agreement is obtained in comparisons between theory and experiments [9,49]. Future work will focus on comparisons of the present theory and ongoing higher resolution experiments with inert gas perturbers [55].

ACKNOWLEDGMENTS

We thank R. Côté and A. Dalgarno for helpful communications, E. Tiemann for generously supplying us with additional unpublished data, and J. P. Woerdman for permission to reproduce experimental data from Ref. [9] in our paper. We are grateful to G. Lister, H. Adler, and W. Lapatovich of OSRAM SYLVANIA, Inc. and M. Shurgalin, W. Parkinson, and K. Yoshino for helpful discussions. This work was supported in part by the National Science Foundation under Grant No. PHY97-24713 and by a grant to the Institute for Theoretical Atomic and Molecular Physics at Harvard College Observatory and the Smithsonian Astrophysical Observatory.

-
- [1] K.K. Verma, J.T. Bahns, A.R. Rajaei-Rizi, and W.C. Stwalley, *J. Chem. Phys.* **78**, 3599 (1983).
- [2] P. Kharchenko, J.F. Babb, and A. Dalgarno, *Phys. Rev. A* **55**, 3566 (1997).
- [3] M. Gutowski, *J. Chem. Phys.* **110**, 4695 (1999).
- [4] A.J. Moerdijk and B.J. Verhaar, *Phys. Rev. A* **51**, R4333 (1995).
- [5] R. Côté and A. Dalgarno, *Phys. Rev. A* **50**, 4827 (1994).
- [6] E. Tiesinga, C. Williams, P.D. Julienne, K.M. Jones, P.D. Lett, and W.D. Phillips, *J. Res. Natl. Inst. Stand. Technol.* **101**, 505 (1996).
- [7] F.A. van Abeelen and B.J. Verhaar, *Phys. Rev. A* **59**, 578 (1999).
- [8] A. Crubellier, O. Dulieu, F. Masnou-Seeuws, H. Knöckel, and E. Tiemann, *Eur. Phys. D* **6**, 211 (1999).
- [9] J. Schlejen, C.J. Jalink, J. Korving, J.P. Woerdman, and W. Müller, *J. Phys. B* **20**, 2691 (1987).
- [10] H.-K. Chung, K. Kirby, and J.F. Babb, *Phys. Rev. A* **60**, 2002 (1999).
- [11] C. Garrod, *Statistical Mechanics and Thermodynamics* (Oxford University Press, New York, 1995).
- [12] K.M. Sando and A. Dalgarno, *Mol. Phys.* **20**, 103 (1971).
- [13] R.O. Doyle, *J. Quant. Spectrosc. Radiat. Transf.* **8**, 1555 (1968).
- [14] L.K. Lam, A. Gallagher, and M.M. Hessel, *J. Chem. Phys.* **66**, 3550 (1977).
- [15] F.H. Mies and P.S. Julienne, *J. Chem. Phys.* **77**, 6162 (1982).
- [16] W.T. Zemke and W.C. Stwalley, *J. Phys. Chem.* **100**, 2661 (1994).
- [17] M. Marinescu, H.R. Sadeghpour, and A. Dalgarno, *Phys. Rev. A* **49**, 982 (1994).
- [18] B.M. Smirnov and M.I. Chibisov, *Zh. Eksp. Teor. Fiz.* **48**, 939 (1965) [*Sov. Phys. JETP* **21**, 624 (1965)].
- [19] K.M. Jones, S. Maleki, S. Bize, P.D. Lett, C.J. Williams, H. Richling, H. Knöckel, E. Tiemann, H. Wang, P.L. Gould, and W.C. Stwalley, *Phys. Rev. A* **54**, R1006 (1996).
- [20] D.D. Konowalow, M.E. Rosenkrantz, and D.S. Hochhauser, *J. Chem. Phys.* **72**, 2612 (1980).
- [21] G. Gerber and R. Möller, *Chem. Phys. Lett.* **113**, 546 (1985).
- [22] E. Tiemann, H. Knöckel, and H. Richling, *Z. Phys. D* **37**, 323 (1996).
- [23] E. Tiemann (private communication).
- [24] M. Marinescu and A. Dalgarno, *Phys. Rev. A* **52**, 311 (1995).
- [25] NIST Atomic Spectroscopic Database, <http://physics.nist.gov/PhysRefData/contents-atomic.html> (1999).
- [26] K.K. Verma, T. Vu, and W.C. Stwalley, *J. Mol. Spectrosc.* **85**, 131 (1981).
- [27] H. Itoh, Y. Fukuda, H. Uchiki, K. Yamada, and M. Matsuoka, *J. Phys. Soc. Jpn.* **52**, 1148 (1983).
- [28] P. Kusch and M.M. Hessel, *J. Chem. Phys.* **68**, 2591 (1978).
- [29] W. Demtröder and M. Stock, *J. Mol. Spectrosc.* **55**, 476 (1975).
- [30] E. Tiemann, *Z. Phys. D* **5**, 77 (1987).
- [31] J. Keller and J. Weiner, *Phys. Rev. A* **29**, 2943 (1984).
- [32] H. Vedder, G. Chawla, and R. Field, *Chem. Phys. Lett.* **111**, 303 (1984).
- [33] J.J. Camacho, J.M.L. Poyato, A.M. Polo, and A. Pardo, *J. Quant. Spectrosc. Radiat. Transf.* **56**, 353 (1996).
- [34] L. Li, S.F. Rice, and R.W. Field, *J. Chem. Phys.* **82**, 1178 (1985).
- [35] E.J. Friedman-Hill and R.W. Field, *J. Chem. Phys.* **96**, 2444 (1992).
- [36] T.-S. Ho, H. Rabitz, and G. Scoles, *J. Chem. Phys.* **112**, 6218 (2000).
- [37] S. Magnier, P. Millié, O. Dulieu, and F. Masnou-Seeuws, *J. Chem. Phys.* **98**, 7 (1993).
- [38] G. Jeung, *J. Phys. B* **16**, 4289 (1983).
- [39] A. Färbert and W. Demtröder, *Chem. Phys. Lett.* **264**, 225 (1997).

- [40] A. Färbert, J. Koch, T. Platz, and W. Demtröder, *Chem. Phys. Lett.* **223**, 546 (1994).
- [41] W.J. Stevens, M.M. Hessel, P.J. Bertocini, and A.C. Wahl, *J. Chem. Phys.* **66**, 1477 (1977).
- [42] D.D. Konowalow, M.E. Rosenkrantz, and D.S. Hochhauser, *J. Mol. Spectrosc.* **99**, 321 (1983).
- [43] T.W. Ducas, M.G. Littman, M.L. Zimmerman, and D. Kleppner, *J. Chem. Phys.* **65**, 842 (1976).
- [44] J.P. Woerdman, *Chem. Phys. Lett.* **53**, 219 (1978).
- [45] G. Baumgartner, H. Kornmeier, and W. Preuss, *Chem. Phys. Lett.* **107**, 13 (1984).
- [46] A. Pardo (unpublished).
- [47] W. Demtröder, W. Stetzenbach, M. Stock, and J. Witt, *J. Mol. Spectrosc.* **61**, 382 (1976).
- [48] J.J. Camacho, J. Santiago, A. Pardo, D. Reyman, and J.M.L. Poyato, *J. Quant. Spectrosc. Radiat. Transf.* **65**, 729 (2000).
- [49] J.P. Woerdman and J.J. de Groot, *Chem. Phys. Lett.* **80**, 220 (1981).
- [50] K.M. Sando and J.C. Wormhoudt, *Phys. Rev. A* **7**, 1889 (1973).
- [51] J. Szudy and W.E. Baylis, *J. Quant. Spectrosc. Radiat. Transf.* **15**, 641 (1975).
- [52] J.J. de Groot, J. Schlejen, J.P. Woerdman, and M.F.M. DeKieviet, *Philips J. Res.* **42**, 87 (1987).
- [53] J.J. de Groot and J.A.J.M. van Vliet, *J. Phys. D* **8**, 651 (1975).
- [54] D. Vežna, J. Rukavina, M. Movre, V. Vujnović, and G. Pichler, *Opt. Commun.* **34**, 77 (1980).
- [55] M. Shurgalin, W.H. Parkinson, K. Yoshino, C. Schoene, and W.P. Lapatovich, *Meas. Sci. Technol.* **11**, 730 (2000).